Journal of Colloid and Interface Science 533 (2019) 182–189

Contents lists available at ScienceDirect

Journal of Colloid and Interface Science

journal homepage: www.elsevier.com/locate/jcis

Regular Article

# Construction of hydrophobic alginate-based foams induced by zirconium ions for oil and organic solvent cleanup

Yaquan Wang, Yi Feng, Jianfeng Yao *

*College of Chemical Engineering, Jiangsu Key Lab for the Chemistry & Utilization of Agricultural and Forest Biomass, Jiangsu Co-Innovation Center of Efficient Processing and Utilization of Forest Resources, Nanjing Forestry University, Nanjing, Jiangsu 210037, China*

## GRAPHICAL ABSTRACT

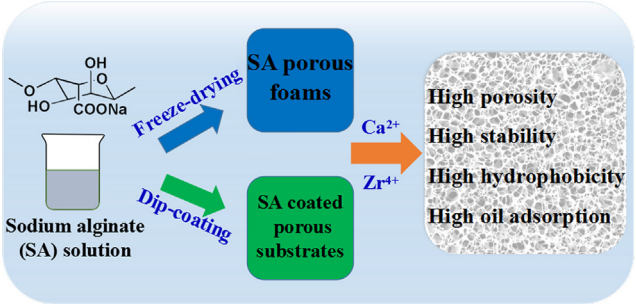


## ARTICLE INFO

*Article history:*
Received 16 July 2018
Revised 14 August 2018
Accepted 22 August 2018
Available online 23 August 2018

*Keywords:*
Sodium alginate
Zirconium ion
Hydrophobic and oleophilic foam
Oil adsorption and cleanup

## ABSTRACT

Hydrophobic modification of sodium alginate (SA) foams via a simple freeze-drying and post cross-linking induced by zirconium (Zr) ions was developed. All results demonstrated that Zr ions not only constructed surface microstructure but also lowered surface energy of foams, leading to the hydrophobic character. Hydrophobic and oleophilic foams showed excellent adsorption capacities for different oils and organic solvents (11.2–25.9 g/g). Furthermore, SA solution can be also coated on porous substrates, such as melamine sponges (MS) and Nylon strainers (NS), to give hydrophobic modification by Zr ion crosslinking. These excellent performances made them a promising for oil adsorption and cleanup.



## 1. Introduction

Water contaminants caused by frequent oil spill or organic contaminants from petrochemical, textile, food, steel and metal finishing, have severely jeopardized animals, plants and human beings [1,2]. To date, numerous strategies such as physical adsorption, in situ combustion, biodegradation, filtration membranes, have been applied to remove oil spills [3,4]. Among them, adsorption is always viewed as a promising technique because of its high efficiency, low cost and easy operation [5,6]. In the past few years, actived carbon, zeolite, clay, and carbon nanotubes have been used as effective adsorbents for oils and organic solvents cleanup [7–9]. However, these traditional composites are powdery and difficult to be separated and recovered in industrial applications [10]. Moreover, they may generate secondary pollutants due to itself leakage, particularly in flowing streams [10,11]. Recently, various wettable materials especially three-dimensional (3D) adsorbent materials have become one of the most attractive materials for oil-spill cleanup [12].

To effectively separate oil from water, oil absorbents possess hydrophobic and oleophilic property [13]. In general, low surface

* Corresponding author.
*E-mail address:* jfyao@njfu.edu.cn (J. Yao).

https://doi.org/10.1016/j.jcis.2018.08.073
0021-9797/

energy and rough micro-/nanostructure were key prerequisites to construct hydrophobic surfaces [14,15]. According to above principle, much significant efforts have been devoted to developing oil adsorbents using common strategies including dip-coating method [16], spray-coating method [17], solvothermal method [18] or in situ growth method [19]. In our previous work, we demonstrated hydrophobic modification of melamine sponge (MS) using poly(furfuryl alcohol), forming a hydrophobic layer via dip-coating method [20]. These as-obtained MS exhibited excellent adsorption capacities for various oils and organic solvents (75–160 g/g). In another typical example, Zhu et al. fabricated superhydrophobic foams with graphene via one-pot thermal reduction method [21]. During the thermal reduction process, reduced graphene oxide (rGO) was self-assembled on 3D skeletons, and thus surface energy and roughness were improved dramatically. Although these extraordinary materials have shown a promise for oil treatment, there are still some challenges and drawbacks to be overcame, such as using expensive modifying agents, slow biodegradability as well as environmental problems caused during the preparation process. In this respect, novel biomass-based oil adsorbents materials have become a rising star because of their extensive sources, renewability and biodegradability [18,22]. As a significant example, Feng et al. prepared centimeter-sized porous carbon spheres oils adsorbent via carbonization of the fruit of Liquidambar formosana [23]. Remarkably, it has been recognized as a good choice to develop hydrophobic biomass-derived adsorbents for oil/water separation applications [24,25].

Sodium alginate (SA) consists of β-(1-4) linked D-mannuronic acid (M unit) and α-(1-4) linked L-guluronic acid (G unit), arranged in blocks aboundant in G units (...GGGGG...), blocks abundant in M units (...MMMMM...), and blocks of alternating G and M units (...GMGMGM...) [26,27]. Furthermore, it is a low-cost, non-toxic, and renewable polysaccharide containing many functional groups (e.g. —COONa and —OH) [28,29]. It can also form hydrogels by ionotropic gelation with divalent ion ($Ca^{2+}$, $Cu^{2+}$, $Pb^{2+}$, $Cd^{2+}$, $Ba^{2+}$) [18,30,31], trivalent ions ($Ce^{3+}$, $Al^{3+}$, $Fe^{3+}$) [32–34], quadrivalent ($Zr^{4+}$) [35,36] and even free metal ions (hydrochloric acid, oxalic acid) [37]. However, the hydrophobicity of SA crosslinked by $Zr^{4+}$ was ignored owing to micron size and oxygen-containing groups. Recently, we have synthesized 3D alginate-based foams via $Ca^{2+}$ crosslinking for heavy metal ions ($Cu^{2+}$, $Cd^{2+}$) removal [38]. Unfortunately, $Ca^{2+}$-induced SA foams were intrinsically amphiphilic absorbents, usually absorbing both water and organic chemicals simultaneously. So it was restricted for selective oil adsorption from water with high efficiency.

In this work, we offered a new strategy to design hydrophobic SA foams for oils adsorption by ionic crosslinking method. Amphoteric SA-Ca foams were crosslinked with Zr ions to improve hydrophobic property. To our knowledge, ion-induced hydrophobicity in SA-Ca foam has not been reported previously. The hydrophobicity of SA-based foams is characterized by Scanning electron microscopy, X-ray photoelectron spectroscopy and Fourier transform infrared spectra. Furthermore, the versatility of SA was demonstrated as well. Hydrophobic performance and oil adsorption capacity of porous substrates, such as MS and Nylon strainers (NS), coated with SA hydrophobic coatings were also investigated.

## 2. Experimental section

### 2.1. Chemicals

Sodium alginate (analytical reagents, SA) was purchased from Sinopharm Chemical, China. Zirconyl chloride octahydrate ($ZrOCl_2 \cdot 8H_2O$) was obtained from Shanghai Titan, China. Anhydrous calcium chloride (analytical reagents, $CaCl_2$) was purchased from Xilong Scientific Co., Ltd., China. Nylon strainers with 180 mesh were obtained from local supermarket. Commercial melamine sponges (LD-1539F, $8 \times 5 \times 2.5\ cm^3$) were bought from Ledian householship store, Zhejiang, China.

### 2.2. Synthesis of sodium alginate-based foams

3D hydrophobic SA foams were fabricated as follows. 1 g of SA was dissolved in 25 ml of deionized water to form clear and viscous slurry. Then SA slurry was injected into a cubic mould with a size of $1 \times 1 \times 1\ cm^3$ by a syringe, followed by lyophilization overnight to prepare SA foams. Subsequently, these obtained SA foams (1 g) were impregnated in 200 ml of $CaCl_2$ solution (5 wt%) and kept for 4 h to develop calcium alginate (SA-Ca) foams. The perpared foams were washed several times with deionized water to remove residual $CaCl_2$ solution. After that, SA-Ca foams were soaked in 200 ml of $ZrOCl_2 \cdot 8H_2O$ solution (3 wt%) and maintained for 4 h for the crosslink reaction at ambient temperature. The resulting foams were obtained after washing until the pH of solution from acidity to neutrality and then freeze-dried again, and it was denoted as SA-Ca-Zr foams. SA-Zr foams were synthesised by the same method as above without using $CaCl_2$ solution.

### 2.3. Characterizations

Surface functional groups of composite materials were detected by a Fourier transform infrared spectra (FTIR) spectrophotometer (Thermo Electron Nicolet-360, USA). The surface morphologies and micro-/nanostructures were recorded by scanning electron microscopy (SEM) utilizing a FEI-Quanta200 (America). Elemental analysis was explored using Energy-dispersive X-ray spectroscopy (EDX) attached to the microscope. Contact angle analysis (JC2000D1, Shanghai Zhongchen Digital Technic Apparatus Co., Ltd., China) was used to measure the surface wettability of samples. The surface chemical bonds was studied with X-ray photoelectron spectroscopy (XPS, AXIS UltraDLD, Japan).

### 2.4. Measurement of porosity of SA-Ca-Zr foams

SA-Ca-Zr foams were completely immersed in absolute ethanol for about 1 min and then removed for measurement [39]. The porosity of SA-Ca-Zr foam was calculated as follows Eq. (1):

$$\text{Porosity}\ (\%) = (m - m_0)/(\rho \times v) \times 100 \quad (1)$$

where $m_0$ (g) and m (g) stand for the mass of foam before and after ethanol saturation, respectively. ρ is the density of absolute ethanol (0.789 g/cm$^3$), and v represents the bulk volume of the SA-Ca-Zr foam.

### 2.5. Oil and organic solvent adsorption

All kinds of organic solvents and oils such as dimethylformamide, *n*-hexane, acetone, chloroform, toluene, tetrachloromethane, paraffin liquid, cyclohexane, ethyl alcohol and soybean oil were employed in this work to evaluate adsorption capacities of modified foams by weighing method. In brief, rectangular foams were preweighed and then immersed in different organic solvents or oils without water for ca. 1 min to reach adsorption equilibrium. After that, these saturated foams were held in air for ca. 1 min to remove excessive oils or solvents before weighing [40]. The adsorption capacity of SA-Ca-Zr foams was calculated according to Eq. (2):

$$Qe = (m - m_0)/m_0 \quad (2)$$

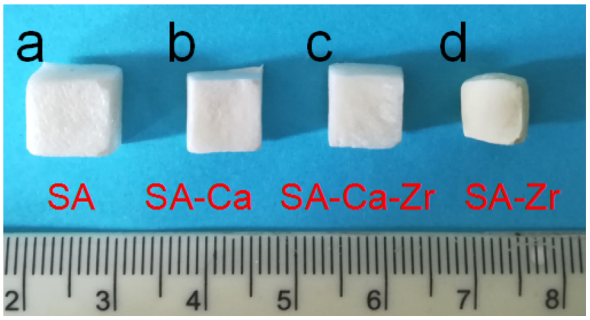


**Fig. 1.** Digital photos of SA, SA-Ca, SA-Ca-Zr and SA-Zr foams (a–d).

where Qe (g/g) is the adsorption capacity of samples at equilibrium; $m_0$ (g) and m (g) are the mass of samples before and after adsorption of various solvents or oils.

3D porous SA-based foams were studied to evaluate their oil/water separation performances by adsorbing soybean oil layer and chloroform droplets (both dyed with Oil Red O) from water, respectively. 3D foams were forced to contact soybean oil and chloroform by tweezers. Meanwhile, the adsorption process of hydrophobic foams was recorded by camera.

The reusability and desorption experiments were also performed as follows. The used foams were gently squeezed several times and washed by absolute ethanol until organic solvents or oils were desorbed from foams completely. Finally, regenerate adsorbents were dried at 80 °C in an oven overnight and utilized for next cycle of adsorption. Additionally, the number of cycles is six times.

## 3. Results and discussion

These hydrophobic SA-based foams were obtained after freeze-drying and ionic crosslinking method. All digital images of SA-based foams are shown in Fig. 1. SA foam has a rectangular shape with a size of 0.9 × 0.9 × 0.6 $cm^3$ (Fig. 1a). The morphologies of SA-Ca and SA-Ca-Zr foams are in the rectangular shape with a size of 0.8 × 0.8 × 0.6 $cm^3$ (Figs. 1b and 1c) while SA-Zr foams displays an irregular shape (0.6 × 0.6 × 0.5 $cm^3$) (Fig. 1d). Volume shrinkage rates of SA-Ca-Zr and SA-Ca foams are ca. 21%, which is much smaller than that of SA-Zr foams (63%). Cross-section morphologies of SA-Ca-Zr and SA-Zr foams were also investigated. SA-Ca-Zr foam has the same inner structure as the exterior surface (Fig. S1a), but SA-Zr foam shows a hole (Fig. S1b), which should arise from the big shrink induced by pure Zr ions. In addition, the porosity of SA-Ca-Zr foams is calculated to be ca. 81.8%, which is quite suitable for adsorption.

Fig. 2 shows SEM images of cross-section and corresponding surface morphologies of SA, SA-Ca, SA-Zr, and SA-Ca-Zr foams with 3D porous structures (Fig. 2a–d). The pore sizes of four SA-based foams are in the range of 30–100 μm, thereby favoring foams to adsorb various oils and organic solvents directly. Fig. 2e and f display that SA and SA-Ca foams have smooth surfaces. SA-Zr and SA-Ca-Zr foams surface with micron-sized protrusions have become much rougher (Fig. 2g and h). According to Cassie theory, surface roughness facilitates the trapping of air, which should be related to the improvement of surface hydrophobicity [41,42].

Fig. 3 displays surface wettability differences between SA-Ca and SA-Ca-Zr foams. When water droplet (colored with methylene blue) and soybean oil droplet (dyed with oil red O) were dropped on the SA-Ca and SA-Ca-Zr foam, both oil and water penetrated into the SA-Ca foam within a short time, proving amphiphilic nature of SA-Ca foams (Fig. 3a). In contrast, the water droplet maintained a stable spherical shape on the foam surface while the soybean oil droplet was quickly absorbed into SA-Ca-Zr foam (Fig. 3b). Even after the SA-Ca-Zr foam was cut into two pieces as shown in Fig. 3c, the new cut surface still maintained superior hydrophobic and oleophilic properties, indicating uniformity of the hydrophobicity on the bulk structure. As shown in Fig. 3d, The water contact angles (WCAs) on SA-Ca-Zr foam surface was 130.4–140.5°. Additionally, the hydrophobic behavior of SA-Ca and SA-Ca-Zr foams is further demonstrated by digital pictures (Fig. 3e and f). After being placed on water surface, the SA-Ca foam soaked beneath the water surface quickly due to the hydrophilic nature. While SA-Ca-Zr foam floated on the water surface without water adsorption, displaying superior water repellence (Fig. 3e). More significantly, when SA-Ca-Zr foam was forced into water by tweezers, the surface of foam was surrounded by air bubbles, resulting in the generation of silver mirror-like surface (Fig. 3f). Once external force was released, hydrophobic SA-Ca-Zr foam floated again. All results demonstrated that SA-Ca-Zr foams possessed highly stable hydrophobicity. SA-Zr foams were also tested and showed hydrophobic and oleophilic as well (Fig. S2).

Benefiting from their hydrophobic properties and interconnected porous structure, SA-Ca-Zr foams have been applied as adsorbents to separate light oil soybean oil and heavy oil chloroform from water. The adsorption process of soybean oil and chloroform droplets (both are dyed with oil red O) is shown in the Fig. 4. A piece of SA-Ca-Zr foam removed soybean oil completely within 15 s when it was placed on the soybean oil layer (Fig. 4a) (Video S1). In addition, SA-Ca-Zr foam could also immediately extract underwater chloroform droplets, which simultaneously

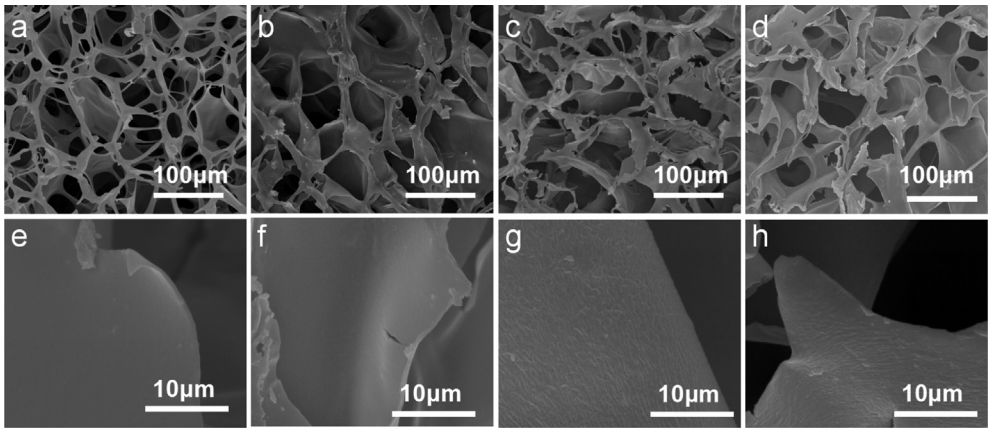


**Fig. 2.** SEM images of cross-section and corresponding surface morphologies of SA (a, e), SA-Ca (b, f), SA-Zr (c, g), and SA-Ca-Zr foam (d, h).

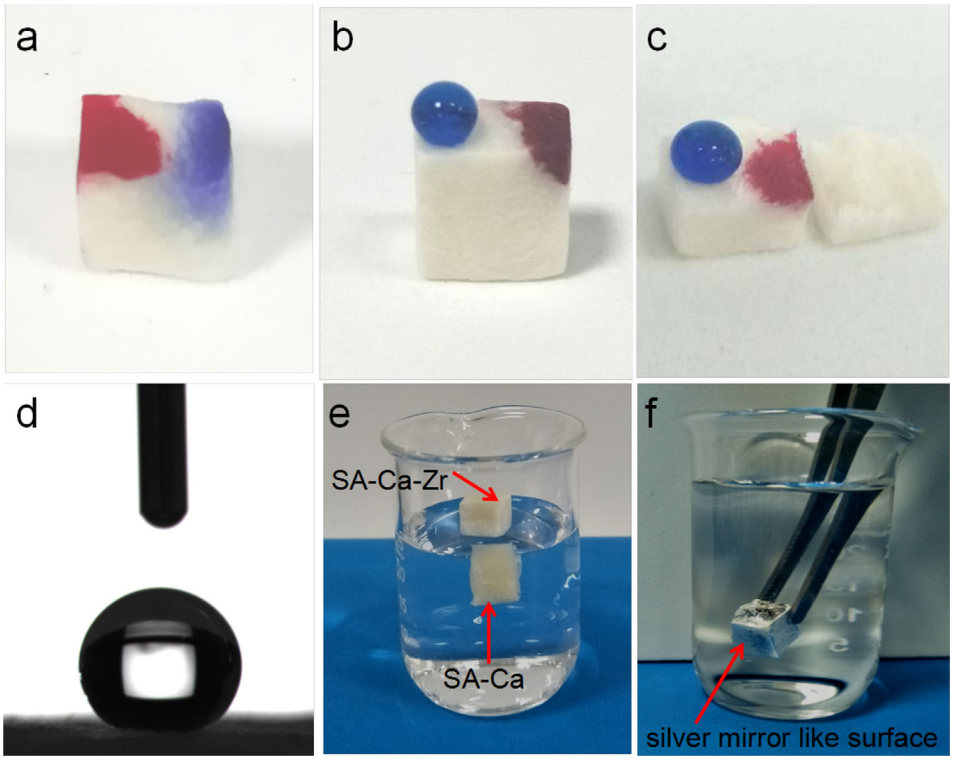


**Fig. 3.** Digital photos of water and oil droplets on SA-Ca (a), SA-Ca-Zr foams (b) and a new cut of the SA-Ca-Zr foam (c), water contact angle of SA-Ca-Zr foam (d), SA-Ca-Zr and SA-Ca foams in water (e), and SA-Ca-Zr foam forced in water (f).

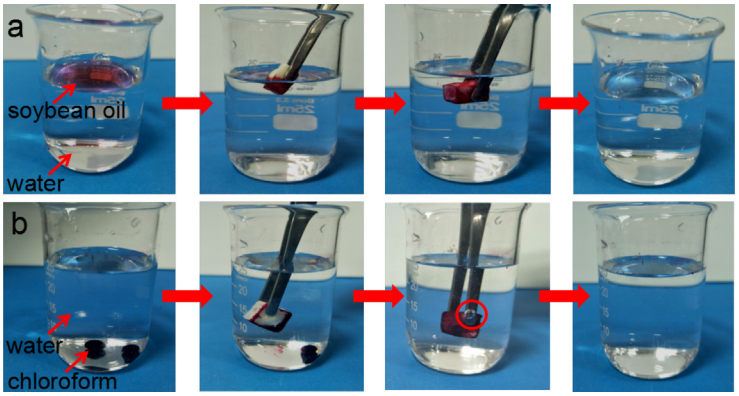


**Fig. 4.** Adsorption of soybean oil floating on the water (a), and chloroform underwater (b) using SA-Ca-Zr foams.

replaced air bubbles to fill the space in a foam when it was immersed into water by external force (Fig. 4b) (Video S2). The hydrophobic and oleophilic performance of SA-Ca-Zr foams resulted from its low surface energy and rough microstructure. These used SA-Ca-Zr foams turned to red and transparent water remained. Based on all facts, it proves that SA-Ca-Zr foams have potential applications for efficient removal of various organic contaminants.

To quantitatively evaluate adsorption performances of SA-Ca-Zr foams, maximum adsorption capacities were measured. In adsorption experiments, ten kinds of pollutants (e.g. dimethylformamide, *n*-hexane, acetone, chloroform, toluene, tetrachloromethane, paraffin liquid, cyclohexane, ethyl alcohol and soybean oil) were selected as adsorbates and foams as adsorbents were subsequently soaked in different oils or organic solvents. SA-Ca-Zr foams showed excellent adsorption capacities of 11.2–25.9 g/g, depending on the density of liquids tested (Fig. 5a). For example, the adsorption of chloroform ($\rho = 1.50\ g/cm^3$) was much higher than that of *n*-hexane ($\rho = 0.65\ g/cm^3$). It is consistent with literature about oils adsorption [43]. However, adsorption capacities of SA-Zr foam for the same contaminants were tested in the range of 3.3–9.3 g/g (Fig. S3). SA-Zr foams demonstrate an inferior adsorption performance to SA-Ca-Zr foams, which should arise from the much denser structure of SA-Zr foams. Notably, adsorption capacities of SA-Ca-Zr foams are relatively higher than other advanced adsorbents and detailed comparisons are listed in Table 1. Compared with other adsorbents that are usually modified by poisonous and expensive modifying agents (trimethylchlorosilane, polydimethylsiloxane) [44,45], toxic reagents (NMP, acetone) [34], the cross-linked method is environmently friendly and can be widely used in the future. Moreover, SA based foams are porous and easily biodegradable, and have a prospect to replace sponges. Therefore, SA-Ca-Zr foams possess advantages over other oil adsorbents for actual removal of organic pollutants.

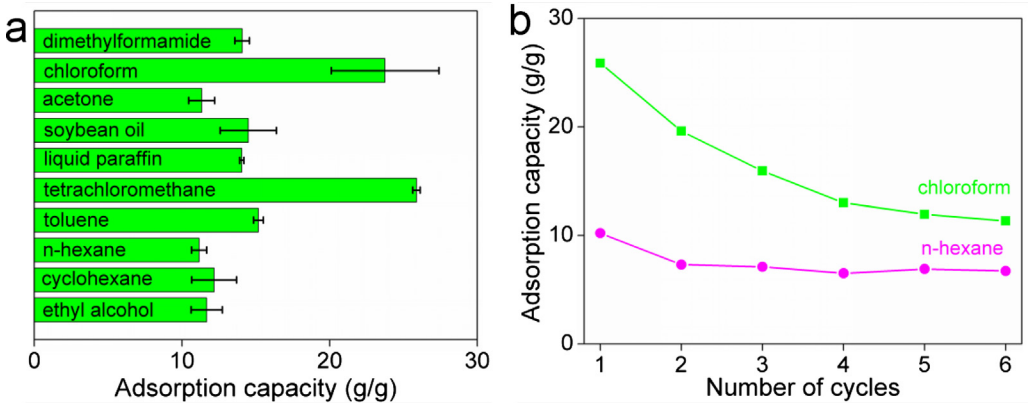


**Fig. 5.** Oil adsorption capacity of SA-Ca-Zr foam (a), and the reusability of SA-Ca-Zr foam for *n*-hexane and chloroform (b).

**Table 1**
Adsorption capacity for oils and organic solvents using different adsorbents.

| Adsorbents | Adsorption capacity (g/g) | Reference |
|---|---|---|
| SA-Ca-Zr foam | 11.2–25.9 | This work |
| SA-Zr foam | 3.3–9.3 | This work |
| Polysulfone microcapsule | 13.8–17.3 | [8] |
| Chitosan/cellulose aerogel | 13.77–28.20 | [45] |
| Wood | 5–15 | [46] |
| Cellulose sponge | 13–18 | [44] |
| Polyhemiaminal aerogels | 7–22 | [34] |
| Lignin/PU sponge | 28.9 (maximum) | [47] |
| Silica aerogel | 10.6 (machine oil) | [48] |
| Poly(lactic acid) materials | 3.5–5 | [49] |

An ideal adsorbents not only have considerable adsorption capacity, but also simultaneously exhibit excellent reusability in practical requirements. From the perspective of density, chloroform and *n*-hexane were chosen as study objects to investigate the reusability of of SA-Ca-Zr foams (Fig. 5b). SA-Ca-Zr foams exhibited adsorption capacities for chloroform and *n*-hexane are 25.3 and 10.2 g/g in the first cycle. After completing six consecutive cycles, the adsorption performance for chloroform decreases by ca. 50%. While the removal efficiency for *n*-hexane decreases by around 30% and remains almost unchanged from the second cycle. It may be explained that pore structures were destroyed and blocked during desorption process [24]. Furthermore, SA-Ca-Zr foams exhibited good stability when they were immersed in the chloroform and toluene for 10 days. The WCAs of SA-Ca-Zr foams as mentioned aboved ranged from 128.8–141.3°. Based on aforementioned analysis, it implies that SA-Ca-Zr foams have an extraordinary recyclability and stability for oils and organic solvents removal.

Viscous SA not only acted as hydrophobic foams via a freeze-drying method but also served as hydrophobic coatings via a dip-coating strategy. To evaluate its versatility, according to our previous work, SA solution was sucessfully supported on the commercial MS for metal ions removal via a in-situ ionic gelation method [50]. On that basis, hydrophobic and oleophilic SA coating can be anchored on porous and amphiprotic substrates, such as MS and NS. Typically, these porous substrates were treated with different concentrations of SA aqueous solution (0.005–0.1 wt%) and resultant hydrophobic materials were prepared after ionic crosslinking (The preparation methods were supplied in details in the supporting information). Additionally, the weight of modified MS and NS could be ignored based on the weight change before and after SA modification. Fig. 6 shows digital photos and surface wettability of the pristine and modified MS and NS. Water droplets (colored with methylene blue) stayed stable spherical

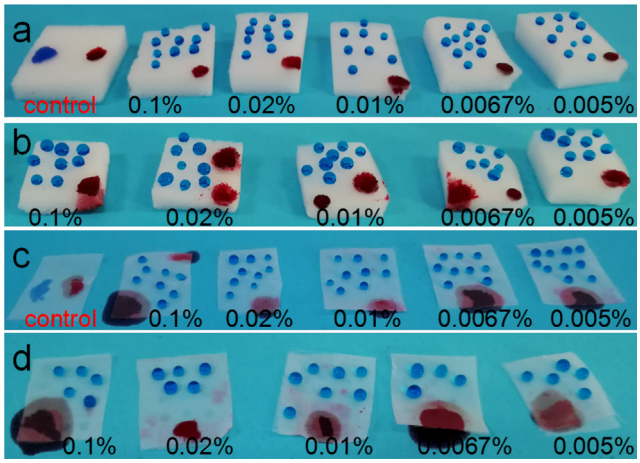


**Fig. 6.** Digital photos of water and oil droplets on the MS/SA-Zr (a), MS/SA-Ca-Zr (b) and the NS/SA-Zr (c), NS/SA-Ca-Zr (d).

shape on the modified MS and NS surfaces while soybean oil (dyed with oil red) was quickly swallowed by the MS and NS. It indicates that MS/SA-Zr, NS/SA-Zr, MS/SA-Ca-Zr, and NS/SA-Ca-Zr composites treated with 0.005–0.1 wt% SA solution have uniform and stable hydrophobic and oleophilic surfaces. The WCAs of MS/SA-Zr, NS/SA-Zr, MS/SA-Ca-Zr, and NS/SA-Ca-Zr composites were ca. 136.7°, 120.5°, 138.7° and 118.8°, respectively (Fig. 7a and Fig. S4a). Besides, hydrophobic MS/SA-Zr and MS/SA-Ca-Zr treated with 0.005 wt% SA solution for oils adsorption were 75.8–159.8 g/g and 73.7–187.7 g/g, respectively (Fig. 7b and Fig. S4b). These results demonstrated that WCAs and adsorption capacities did not rely on the concentrations of SA solution. Therefore, the method for preparation of the hydrophobic coatings on the MS and NS is simple, green, and effective.

## 4. Discussion

SA-Ca foams were obtained by an ion-exchange mechanism between —COONa/$Ca^{2+}$ [51]. Similarly, SA-Zr foams were prepared after crosslinking with $Zr^{4+}$. EDX demonstrated that Na element disappeared and a large quantity of Zr element remained for SA-Zr foams (Fig. S5a) [52]. However, volume shrinkage rates and porosities of SA-Zr and SA-Ca were obviously different, which attributed to the radii of cross-linking ions. As the radius of the Zr ion (0.72 Å) is much smaller than Ca ion (1.0 Å) [53,54]. Namely, SA polymer chains became more ordered arrangement as the cross-linking ion size increased, and caused the relatively regular

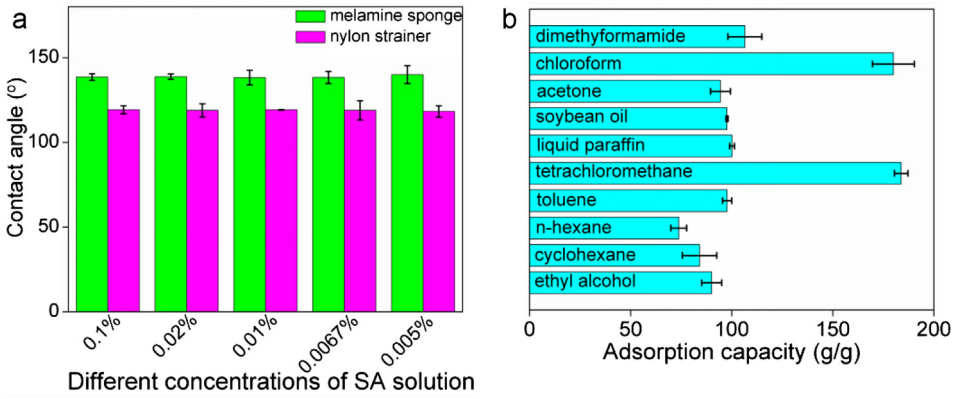


**Fig. 7.** Water contact angles of MS/SA-Ca-Zr and NS/SA-Ca-Zr coated with different concentration of SA solution (a), and oil adsorption capacities of MS/SA-Ca-Zr (b).

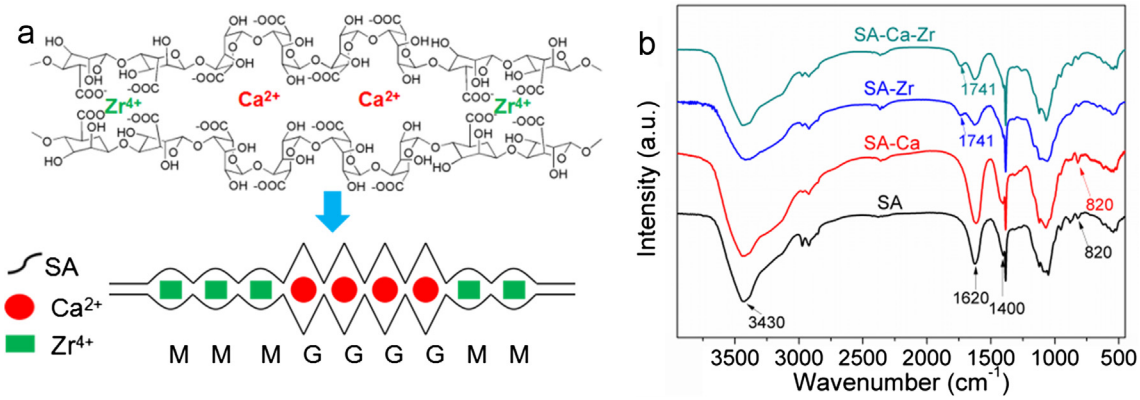


**Fig. 8.** Schematics of SA-Ca-Zr foams crosslinked with $Ca^{2+}$ and $Zr^{4+}$ (a) and FTIR spectra of SA, SA-Ca, SA-Zr, and SA-Ca-Zr foams (b).

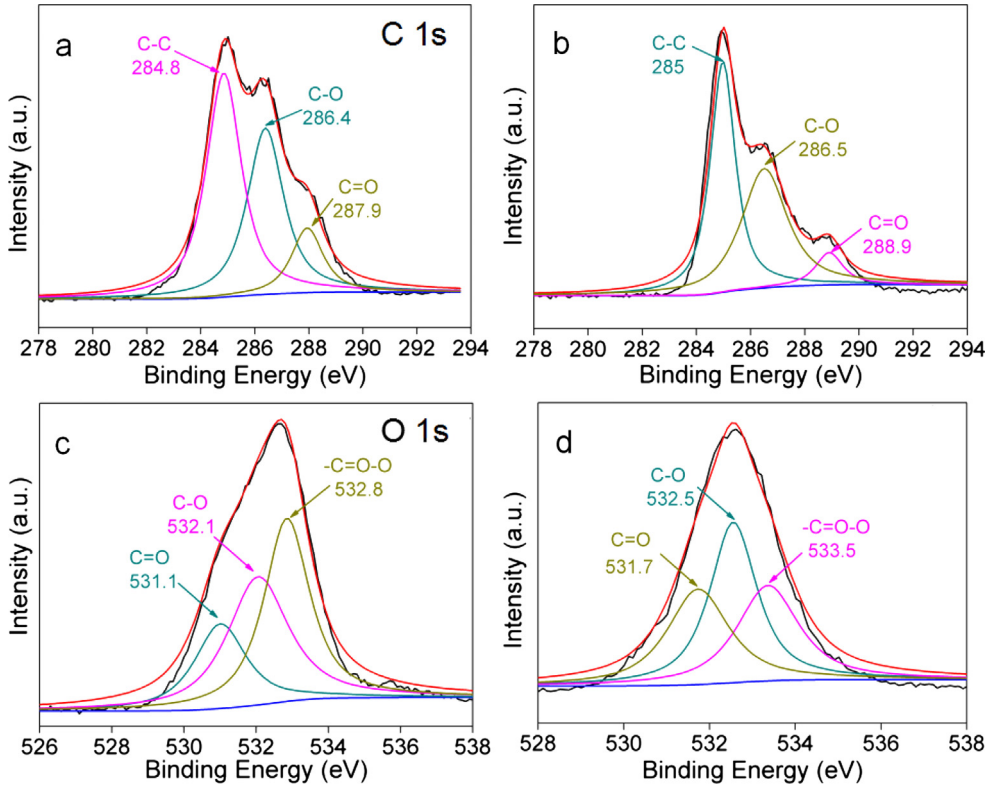


**Fig. 9.** XPS spectra: C 1s peak of SA and the SA-Ca-Zr foams (a, b), O 1s peak of SA and the SA-Ca-Zr foams (c, d).

shape of SA-Ca foams [55]. Noticeably, divalent Ca ions solely bound to G units of SA chains to form "egg-box" structure [56,57]. More interestingly, Zr and Ca elements were coexistent in SA-Ca-Zr foams (Fig. S5a–c), which proved that Zr ions showed affinity for both G and M segments according to analyses mentioned above as well. The process can be described in Fig. 8a. It is worth noting that Zr ions mainly caused the hydrophobic SA composite foam while Ca ions assisted SA foams with more porous structure. Therefore, to achieve high porosity of hydrophobic foams, the SA-based foams should be fabricated by pre-treatment with $CaCl_2$ solution and hydrophobic post-treatment with Zr ion solution.

FTIR analyses of SA, SA-Ca, SA-Zr and SA-Ca-Zr foams were conducted to understand the hydrophobic mechanism of SA-Ca-Zr foams (Fig. 8b). In terms of pristine SA, the sharp and wide absorption peak around 3430 $cm^{-1}$ was corresponded to O-H bonds. In addition, characteristic peaks of SA at 1620 $cm^{-1}$ and 1400 $cm^{-1}$ were attributed to asymmetric and symmetric vibration peak of carboxyl groups (—COOH), respectively [18,58]. After SA crosslinking with $Ca^{2+}$, peak intensity was enhanced at 820 $cm^{-1}$ [59]. Additionally, we also further discuss later, the increased intensity was attributed to the interaction between $Ca^{2+}$ and sodium alginate by XPS. The new band at 1741 $cm^{-1}$ appeared and peak intensity at 1620 $cm^{-1}$ was obviously decreased, suggesting that might associate with the combination of $—COO^-$ and $Zr^{4+}$ by chemical crosslinking according to previous similar study [30,60]. Furthermore, the intensity of peaks at 3430 $cm^{-1}$ in SA-Zr and SA-Ca-Zr foams were decreased. All analyses indicated that surface polarity of SA-based foam (—COOH and —OH) was reduced, supporting that SA-Zr and SA-Ca-Zr foams became hydrophobic and oleophilic.

To further confirm the mechanism of hydrophobicity of SA-based foams, XPS was used to analyze chemical bonds in the SA, SA-Ca, SA-Zr, and SA-Ca-Zr foams. XPS spectra of C 1 s and O 1 s regions of SA-based foams are shown in Fig. 9 and Fig. S6. The C 1 s peaks located at the binding energy of 284.8, 286.4, and 287.9 eV were assigned to C—C, C—O, and C═O bonds, respectively (Fig. 9a) [30]. After the crosslink reaction, typical peak at 287.9 eV (C═O) showed a shift to higher binding energy (288.9 eV) in SA-Ca-Zr (Fig. 9b). In addition, the peaks at 531.1 and 532.8 eV in the O 1s spectrum of SA shifted to 531.7 eV and 533.5 eV in SA-Ca-Zr (Fig. 9c and d) [61]. SA-Ca and SA-Zr foams show similar results (Fig. S6). Actually, surface energy is proportional to surface polarity [62]. These results were corresponded to the aforementioned FTIR analysis and clearly proved that chemical interactions were formed between the metal ions and $—COO^-$, improving surface polarity and resulting in hydrophobic surface.

## 5. Conclusion

The hydrophobic and oleophilic SA-based foam was fabricated via freeze-drying and post cross-linking induced by Zr ions. SEM, FTIR and XPS results indicated that the coordination between carboxyl, hydroxy groups of SA and Zr ions, which not only caused surface roughness but also lowered surface energy of modified foams. So the as-prepared SA-based foam exhibited excellent adsorption capacity of 11.2–25.9 g/g for oils and organic solvents, much higher than recently reported biomass-based adsorbents [44,46]. Meanwhile, hydrophobic SA coating materials can be deposited on melamine sponges and nylon strainers to endow their hydrophobic and oleophilic properties. Furthermore, our work has important industrial and environmental relevance such as (i) renewability and biodegradability of SA, (ii) the use of non-toxic chemicals, and (iii) low-cost raw materials. Moreover, the preparation method of SA-based foams and composites was simple, economic, and scalable, and thus has a high promise for oil spill recovery.

## Acknowledgement

The authors are grateful for the financial support of Natural Science Key Project of the Jiangsu Higher Education Institutions (15KJA220001), Jiangsu Province Six Talent Peaks Project (2016-XCL-043). YF thanks the financial support of the Natural Science Foundation of Jiangsu Province Youth Fund (BK20170919).

## Appendix A. Supplementary material

Supplementary data associated with this article can be found, in the online version, at https://doi.org/10.1016/j.jcis.2018.08.073.

## References

[1] Y. Zhu, D. Chen, Novel clay-based nanofibrous membranes for effective oil/water emulsion separation, Ceram. Int. 43 (2017) 9465–9471.
[2] H. Ji, R. Zhao, Y. Li, B. Sun, Y. Li, N. Zhang, J. Qiu, X. Li, C. Wang, Robust and durable superhydrophobic electrospun nanofibrous mats via a simple Cu nanocluster immobilization for oil-water contamination, Colloid. Surface. A. 538 (2018) 173–183.
[3] A. Turco, E. Primiceri, M. Frigione, G. Maruccio, C. Malitesta, An innovative, fast and facile soft-template approach for the fabrication of porous PDMS for oil-water separation, J. Mater. Chem. A 5 (2017) 23785–23793.
[4] X. Zhao, Y. Su, Y. Liu, Y. Lip, Z. Jiang, Free-standing graphene oxide-palygorskite nanohybrid membrane for oil / water separation, ACS Appl. Mater. Interfaces 8 (2016) 8247–8256.
[5] Q. Liang, H. Luo, J. Geng, J. Chen, Facile one-pot preparation of nitrogen-doped ultra-light graphene oxide aerogel and its prominent adsorption performance of Cr (VI), Chem. Eng. J. 338 (2018) 62–71.
[6] X. Zheng, X. Xiong, J. Yang, D. Chen, R. Jian, L. Lin, A strong and compressible three dimensional graphene/polyurushiol composite for efficient water cleanup, Chem. Eng. J. 333 (2018) 153–161.
[7] H.-J. Song, X.-Q. Shen, X.-F. Meng, Superhydrophobic surfaces produced by carbon nanotube modified polystyrene composite coating, J. Disper. Sci. Technol. 31 (2010) 1465–1468.
[8] Y. Pan, J. Wang, C. Sun, X. Liu, H. Zhang, Fabrication of highly hydrophobic organic-inorganic hybrid magnetic polysulfone microcapsules: A lab-scale feasibility study for removal of oil and organic dyes from environmental aqueous samples, J. Hazard. Mater. 309 (2016) 65–76.
[9] V. Rajakovic-Ognjanovic, G. Aleksic, L. Rajakovic, Governing factors for motor oil removal from water with different sorption materials, J. Hazard. Mater. 154 (2008) 558–563.
[10] C. Shi, C. Lv, L. Wu, X. Hou, Porous chitosan/hydroxyapatite composite membrane for dyes static and dynamic removal from aqueous solution, J. Hazard. Mater. 338 (2017) 241–249.
[11] Y. Li, F. Liu, B. Xia, Q. Du, P. Zhang, D. Wang, Z. Wang, Y. Xia, Removal of copper from aqueous solution by carbon nanotube/calcium alginate composites, J. Hazard. Mater. 177 (2010) 876–880.
[12] W. Lv, Q. Mei, J. Xiao, M. Du, Q. Zheng, 3D multiscale superhydrophilic sponges with delicately designed pore size for ultrafast oil/water separation, Adv. Funct. Mater. 27 (2017) 1704293.
[13] Z. Xue, Y. Cao, N. Liu, L. Feng, L. Jiang, Special wettable materials for oil/water separation, J. Mater. Chem. A 2 (2014) 2445–2460.
[14] J. Ge, H.Y. Zhao, H.W. Zhu, J. Huang, L.A. Shi, S.H. Yu, Advanced sorbents for oil-spill cleanup: recent advances and future perspectives, Adv. Mater. 28 (2016) 10459–10490.
[15] Q. Ma, H. Cheng, A.G. Fane, R. Wang, H. Zhang, Recent development of advanced materials with special wettability for selective oil/water separation, Small 12 (2016) 2186–2202.
[16] R. Cai, K. Glinel, D. De Smet, M. Vanneste, N. Mannu, B. Kartheuser, B. Nysten, A.M. Jonas, Environmentally friendly super-water-repellent fabrics prepared from water-based suspensions, ACS Appl. Mater. Interfaces 10 (2018) 15346–15351.
[17] J. Li, L. Yan, H. Li, J. Li, F. Zha, Z. Lei, A facile one-step spray-coating process for the fabrication of a superhydrophobic attapulgite coated mesh for use in oil/water separation, RSC Adv. 5 (2015) 53802–53808.
[18] H.-Y. Mi, X. Jing, H.-X. Huang, X.-F. Peng, L.-S. Turng, Superhydrophobic graphene/cellulose/silica aerogel with hierarchical structure as superabsorbers for high efficiency selective oil absorption and recovery, Ind. Eng. Chem. Res. 57 (2018) 1745–1755.
[19] Z. Lei, Y. Deng, C. Wang, Multiphase surface growth of hydrophobic ZIF-8 on melamine sponge for excellent oil/water separation and effective catalysis in a Knoevenagel reaction, J. Mater. Chem. A 6 (2018) 3258–3263.
[20] Y. Feng, Y. Wang, Y. Wang, J. Yao, Furfuryl alcohol modified melamine sponge for highly efficient oil spill clean-up and recovery, J. Mater. Chem. A 5 (2017) 21893–21897.
[21] H. Zhu, D. Chen, W. An, N. Li, Q. Xu, H. Li, J. He, J. Lu, A robust and cost-effective superhydrophobic graphene foam for efficient oil and organic solvent recovery, Small 11 (2015) 5222–5229.

[22] F. Jiang, Y.-L. Hsieh, Amphiphilic superabsorbent cellulose nanofibril aerogels, J. Mater. Chem. A 2 (2014) 6337–6342.
[23] Y. Feng, S. Liu, G. Liu, J. Yao, Facile and fast removal of oil through porous carbon spheres derived from the fruit of Liquidambar formosana, Chemosphere 170 (2017) 68–74.
[24] J. Jiang, Q. Zhang, X. Zhan, F. Chen, Renewable, biomass-derived, honeycomblike aerogel as a robust oil absorbent with two-way reusability, ACS Sustain. Chem. Eng. 5 (2017) 10307–10316.
[25] Y. Lu, Y. Wang, L. Liu, W. Yuan, Environmental-friendly and magnetic/silanized ethyl cellulose sponges as effective and recyclable oil-absorption materials, Carbohydr. Polym. 173 (2017) 422–430.
[26] S. Kondaveeti, P.V. de Assis Bueno, A.M. Carmona-Ribeiro, F. Esposito, N. Lincopan, M.R. Sierakowski, D.F. Siqueira Petri, Microbicidal gentamicin-alginate hydrogels, Carbohydr. Polym. 186 (2018) 159–167.
[27] J.-Y. Sun, X. Zhao, W.R.K. Illeperuma, O. Chaudhuri, K.H. Oh, D.J. Mooney, J.J. Vlassak, Z. Suo, Highly stretchable and tough hydrogels, Nature 489 (2012) 133–136.
[28] X. Zhao, G. Yu, J. Li, Y. Feng, L. Zhang, Y. Peng, Y. Tang, L. Wang, Eco-Friendly Pickering Emulsion Stabilized by Silica Nanoparticles Dispersed with High-Molecular-Weight Amphiphilic Alginate Derivatives, ACS Sustain. Chem. Eng. 6 (2018) 4105–4114.
[29] Z.-J. Shao, X.-L. Huang, F. Yang, W.-F. Zhao, X.-Z. Zhou, C.-S. Zhao, Engineering sodium alginate-based cross-linked beads with high removal ability of toxic metal ions and cationic, Carbohydr. Polym. 187 (2018) 85–93.
[30] F. Wang, X. Lu, X.-Y. Li, Selective removals of heavy metals ($Pb^{2+}$, $Cu^{2+}$, and $Cd^{2+}$) from wastewater by gelation with alginate for effective metal recovery, J. Hazard. Mater. 308 (2016) 75–83.
[31] M. Bajpai, P. Shukla, S.K. Bajpai, Ca (II) plus Ba (II) ions crosslinked alginate gels prepared by a novel diffusion through dialysis tube (DTDT) approach and preliminary BSA release study, Polym. Degrada. Stabil. 134 (2016) 22–29.
[32] R.P. Narayanan, G. Melman, N.J. Letourneau, N.L. Mendelson, A. Melman, Photodegradable iron (III) cross-linked alginate gels, Biomacromolecules 13 (2012) 2465–2471.
[33] H. Kaygusuz, F.B. Erim, O. Pekcan, G.A. Evingur, Cation effect on slow release from alginate beads: a fluorescence study, J. Fluoresc. 24 (2014) 161–167.
[34] H. Kaygusuz, E. Torlak, G. Akm-Evingur, I. Ozen, R. von Klitzing, F.B. Erim, Antimicrobial cerium ion-chitosan crosslinked alginate biopolymer films: A novel and potential wound dressing, Int. J. Biol. Macromol. 105 (2017) 1161–1165.
[35] X. Li, Y. Qi, Y. Li, Y. Zhang, X. He, Y. Wang, Novel magnetic beads based on sodium alginate gel crosslinked by zirconium (IV) and their effective removal for $Pb^{2+}$ in aqueous solutions by using a batch and continuous systems, Bioresour. Technol 142 (2013) 611–619.
[36] S.M. Prabhu, S. Meenakshi, Novel one-pot synthesis of dicarboxylic acids mediated alginate-zirconium biopolymeric complex for defluoridation of water, Carbohydr. Polym. 120 (2015) 60–68.
[37] M.M. Perez-Madrigal, J. Torras, J. Casanovas, M. Haering, C. Aleman, D. Diaz Diaz, Paradigm shift for preparing versatile $M^{2+}$-free gels from unmodified sodium alginate, Biomacromolecules 18 (2017) 2967–2979.
[38] Y. Wang, Y. Feng, X.-F. Zhang, X. Zhang, J. Jiang, J. Yao, Alginate-based attapulgite foams as efficient and recyclable adsorbents for the removal of heavy metals, J. Colloid Interface Sci. 514 (2018) 190–198.
[39] N. Lin, C. Bruzzese, A. Dufresne, TEMPO-oxidized nanocellulose participating as crosslinking aid for alginate-based sponges, ACS Appl. Mater. Interfaces 4 (2012) 4948–4959.
[40] M. Khosravi, S. Azizian, Synthesis of a novel highly oleophilic and highly hydrophobic sponge for rapid oil spill cleanup, ACS Appl. Mater. Interfaces 7 (2015) 25326–25333.
[41] P. Phanthong, P. Reubroycharoen, S. Kongparakul, C. Samart, Z. Wang, X. Hao, A. Abudula, G. Guan, Fabrication and evaluation of nanocellulose sponge for oil/water separation, Carbohydr. Polym. 190 (2018) 184–189.
[42] Y. Cai, Q. Lu, X. Guo, S. Wang, J. Qiao, L. Jiang, Salt-tolerant superoleophobicity on alginate gel surfacesinspired by seaweed (Saccharina japonica), Adv. Mater. 27 (2015) 4162–4168.
[43] O. Oribayo, Q. Pan, X. Feng, G.L. Rempel, Hydrophobic surface modification of FMSS and its application as effective sorbents for oil spill clean-ups and recovery, AICHE J 63 (2017) 4090–4102.
[44] M. Xu, G. Wang, Z. Zeng, J. Chen, X. Zhang, L. Wang, W. Song, Q. Xue, Diverse wettability of superoleophilicity and superoleophobicity for oil spill cleanup and recycling, Appl. Surf. Sci. 426 (2017) 1158–1166.
[45] Z. Li, L. Shao, W. Hu, T. Zheng, L. Lu, Y. Cao, Y. Chen, Excellent reusable chitosan/cellulose aerogel as an oil and organic solvent absorbent, Carbohydr. Polym. 191 (2018) 183–190.
[46] Q. Fu, F. Ansari, Q. Zhou, L.A. Berglund, Wood nanotechnology for strong, mesoporous, and hydrophobic biocomposites for selective separation of oil/water mixtures, ACS Nano 12 (2018) 2222–2230.
[47] O.S.H. Santos, M.C. da Silva, V.R. Silva, W.N. Mussel, M.I. Yoshida, Polyurethane foam impregnated with lignin as a filler for the removal of crude oil from contaminated water, J. Hazard. Mater. 324 (2017) 406–413.
[48] M. Li, H. Jiang, D. Xu, Preparation of sponge-reinforced silica aerogels from tetraethoxysilane and methyltrimethoxysilane for oil/water separation, Mater. Res. Express. 5 (2018) 045003.
[49] Z. Xue, Z. Sun, Y. Cao, Y. Chen, L. Tao, K. Li, L. Feng, Q. Fu, Y. Wei, Superoleophilic and superhydrophobic biodegradable material with porous structures for oil absorption and oil-water separation, RSC Adv. 3 (2013) 23432–23437.
[50] Y. Feng, Y. Wang, Y. Wang, X.-F. Zhang, J. Yao, In-situ gelation of sodium alginate supported on melamine sponge for efficient removal of copper ions, J. Colloid Interface Sci. 512 (2018) 7–13.
[51] Y. Ge, X. Cui, C. Liao, Z. Li, Facile fabrication of green geopolymer/alginate hybrid spheres for efficient removal of Cu (II) in water: Batch and column studies, Chem. Eng. J. 311 (2017) 126–134.
[52] V. Gopalakannan, N. Viswanathan, One pot synthesis of metal ion anchored alginate-gelatin binary biocomposite for efficient Cr (VI) removal, Int. J. Biol. Macromol. 83 (2016) 450–459.
[53] M.K. Sharif, M.A. Khan, A. Hussain, F. Iqbal, I. Shakir, G. Murtaza, M.N. Akhtar, M. Ahmad, M.F. Warsi, Synthesis and characterization of Zr and Mg doped $BiFeO_3$ nanocrystalline multiferroics via micro emulsion route, J. Alloy. Compd. 667 (2016) 329–340.
[54] C.H. Yang, M.X. Wang, H. Haider, J.H. Yang, J.-Y. Sun, Y.M. Chen, J. Zhou, Z. Suo, Strengthening alginate/polyacrylamide hydrogels using various multivalent cations, ACS Appl. Mater. Interfaces 5 (2013) 10418–10422.
[55] J. Brus, M. Urbanova, J. Czernek, M. Pavelkova, K. Kubova, J. Vyslouzil, S. Abbrent, R. Konefal, J. Horsky, D. Vetchy, J. Vyslouzil, P. Kulich, Structure and dynamics of alginate gels cross-linked by polyvalent ions probed via solid state NMR spectroscopy, Biomacromolecules 18 (2017) 2478–2488.
[56] C.H. Goh, P.W.S. Heng, L.W. Chan, Alginates as a useful natural polymer for microencapsulation and therapeutic applications, Carbohydr. Polym. 88 (2012) 1–12.
[57] K.Y. Lee, D.J. Mooney, Alginate: Properties and biomedical applications, Prog. Polym. Sci. 37 (2012) 106–126.
[58] I.B. Obot, I.B. Onyeachu, A.M. Kumar, Sodium alginate: A promising biopolymer for corrosion protection of API X60 high strength carbon steel in saline medium, Carbohydr. Polym. 178 (2017) 200–208.
[59] Z. Li, Y. Ge, L. Wan, Fabrication of a green porous lignin-based sphere for the removal of lead ions from aqueous media, J. Hazard. Mater. 285 (2015) 77–83.
[60] R.F.N. Quadrado, A.R. Fajardo, Fast decolorization of azo methyl orange via heterogeneous Fenton and Fenton-like reactions using alginate-$Fe^{2+}$ /$Fe^{3+}$ films as catalysts, Carbohydr. Polym. 177 (2017) 443–450.
[61] Z.-H. Hu, A.M. Omer, X.-K. Ouyang, D. Yu, Fabrication of carboxylated cellulose nanocrystal/sodium alginate hydrogel beads for adsorption of Pb (II) from aqueous solution, Int. J. Biol. Macromol. 108 (2018) 149–157.
[62] Y. Tian, L. Jiang, Wetting intrinsically robust hydrophobicity, Nat. Mater. 12 (2013) 291–292.